ChemComm

COMMUNICATION

View Article Online
View Journal

Cite this: DOI: 10.1039/c9cc02967b

A self-assembled peptidic nanomillipede to fabricate a tuneable hybrid hydrogel†

Jianhui Liu, [a] Rong Ni [ab] and Ying Chau *[a]

Received 16th April 2019,
Accepted 20th May 2019

DOI: 10.1039/c9cc02967b

rsc.li/chemcomm

A peptidic 'nanomillipede', consisting of a worm-like nanoscale 'body' and cysteine-terminated 'legs', was synthesized, tuned (with ultrasound) and utilized to crosslink the vinyl sulfone-modified dextran to form hybrid hydrogels with soft-tissue mimicking tuneable mechanical strength, self-healing property, and tuneable shear-thinning property, thereby indicating its potential use in tissue engineering and drug delivery.

Hydrogels are widely used as a synthetic extracellular matrix (ECM) to integrate cells into a well-defined 3D structure.[1] Cells are responsive to multiple stimuli from the ECM, and appropriate mechanical properties are essential to stimulate the desired cell growth.[2,3] Many investigations have been carried out to tune the mechanical properties of hydrogels, such as changing the polymer concentration,[4] varying the crosslinking molecule concentration[5] or altering the strength of the crosslinked hydrogel network.[6] These methods incorporate either composition change (content of the individual chemical) or component change (incorporation of new materials). Rarely, the properties of crosslinkers within the hydrogel, including their size and geometry, have been investigated. We intend to study here the relationship between the microscopic crosslinker properties and macroscopic hydrogel mechanical properties.

The self-assembled oligopeptide nanostructures provide flexibility to construct biocompatible materials with tuneable properties.[7,8] A polymer–peptide hybrid hydrogel is a representative, which can mimic the natural ECM bioenvironment, while providing soft tissue-mimicking mechanical strength[9] (*e.g.* liver and kidney tissues[10]), feasibility of fabrication[11] and tuneable mechanical properties.[12] A previously reported method to prepare peptide-based hydrogels involves construction of peptide-grafted polymers or peptide block copolymers which further self-assemble into a hybrid hydrogel network.[13,14] With this approach, however, the self-assembling process may be hindered by the polymer backbone and the self-assembling peptide (SAP) structure cannot be readily controlled.[15] To finely tune the peptide nanostructure, we took a different approach in this work. The hydrogel formation started with the preparation of a peptidic nanomillipede crosslinker, which is based on the co-assembly of a normal nanomillipede-forming self-assembling peptide (n_NSAP) and a cysteine-terminated nanomillipede-forming self-assembling peptide (c_NSAP). Next, ultrasound was introduced to tune the length of the nanomillipedes without changing the chemical components and the density of the reaction sites for crosslinking. This control of the crosslinker length can further result in mechanical tuning within the hybrid hydrogel system (Fig. 1). We hypothesize that the 'bottom-up' fabrication of hybrid hydrogels and mechanical tuning through the SAP nanoscale crosslinkers (assisted with ultrasound treatment) can provide a new venue to design macroscopic hydrogel properties, namely, by leveraging the control of the crosslinker nanostructure.

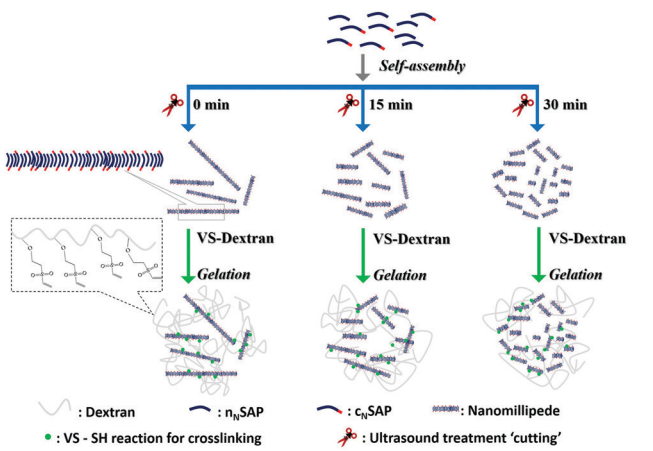

Fig. 1 Schematic illustration of tuneable dextran/peptidic nanomillipede hybrid hydrogel preparation.

[a] Department of Chemical and Biological Engineering, the Hong Kong University of Science and Technology, Clear Water Bay, Kowloon, Hong Kong. E-mail: ying.chau@ust.hk

[b] Institute for Advanced Study, the Hong Kong University of Science and Technology, Clear Water Bay, Kowloon, Hong Kong

† Electronic supplementary information (ESI) available: Supplementary figures, tables and experimental procedures. See DOI: 10.1039/c9cc02967b

A thiol-containing peptidic 'nanomillipede' was prepared by the co-incubation of n_NSAP and c_NSAP (Fig. S1–S7, ESI†). It mimics the millipede in terms of the high aspect ratio and self-regenerative function, which will be further discussed. The growth of the nanomillipede was characterized by atomic force microscopy (AFM) and transmission electron microscopy (TEM). The freshly prepared low aspect-ratio nanorods (Fig. S8, ESI†) mature axially into high aspect-ratio worm-like nanomillipedes after 48 h of incubation (Fig. 2a, b and Fig. S9, ESI†). Attenuated total reflectance Fourier-transform infrared spectroscopy (ATR-FTIR) was used to characterize the peptide secondary structure within nanomillipedes (Fig. S10, ESI†). The band of 1625 cm^{-1} (amide I stretch peak) and the shoulder of 1695 cm^{-1} indicate the antiparallel β-sheet architecture.[16] The β-sheet secondary structure was further confirmed by the circular dichroism (CD) spectrum, showing a positive peak around 198 nm and a negative peak around 215 nm (Fig. S11, ESI†). The negative shoulder peak at 228 nm represents a tryptophan (W)-containing self-assembling peptide.[17] A scrambled self-assembling peptide (SAP) mixture consisting of sn_NSAP and sc_NSAP was also prepared as the negative control (Fig. S1–S7, ESI†). The presence of a disordered random coil structure was confirmed by both ATR-FTIR[18] (Fig. S12, ESI†) and CD spectra (Fig. S13, ESI†).[19] Tryptophan fluorescence measurement was carried out to monitor the structural change during the self-assembly. For both the nanomillipede and the scrambled SAP mixture, the fluorescence intensity reached a plateau after 48 hour incubation (Fig. S14, ESI†). The fluorescence intensity of the tryptophan probe is highly environment dependent, which is used to characterize the hydrophobic interaction driven self-assembling process of the peptide or protein folding.[20] Compared with the scrambled SAP mixture, the tryptophan residues within the nanomillipede displayed a higher fluorescence intensity with blue-shifted maximal emission wavelengths (from 348 nm to 343 nm) (Fig. S15, ESI†), which is in agreement with the fact that tryptophan residues within the nanomillipede buried in the more hydrophobic environment than those within the scrambled SAP. These structural characterization data imply that n_NSAP and c_NSAP co-assembled into an ordered β-sheet secondary structure, which constructed a nanomillipede architecture with a high aspect ratio.

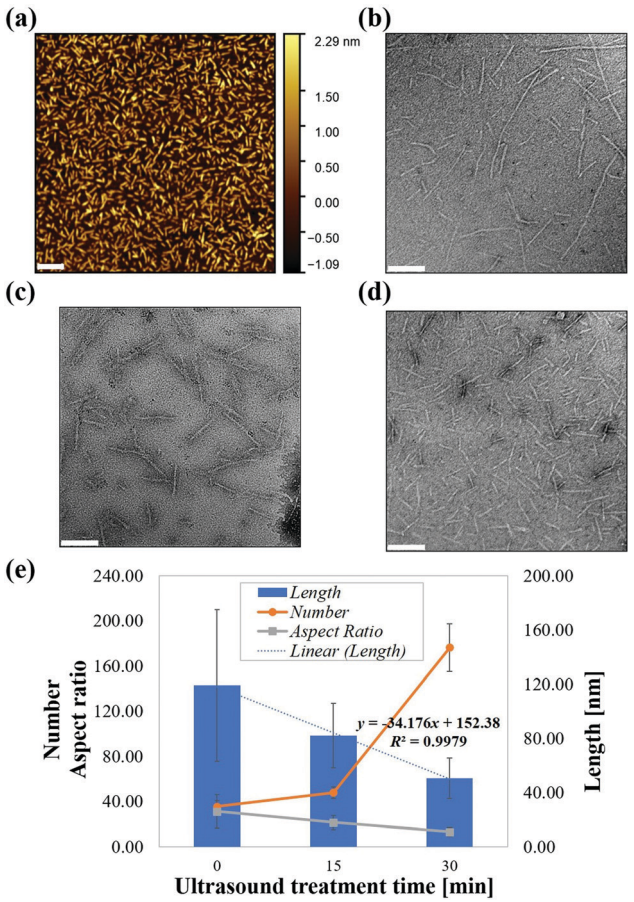

Fig. 2 Structural characterization of peptide nanomillipedes. (a) AFM image. Scale bar: 200 nm. The TEM images of nanomillipedes treated with (b) 0 min (c) 15 min and (d) 30 min. Scale bar: 100 nm. (e) Quantitative analysis.

The length of the peptidic nanomillipede could be well-tuned through varying the duration of ultrasound treatment. Ultrasound can transmit energy *via* liquid (peptide buffer solution) to cause a localized pressure change, where the intermolecular interactions can be broken, essentially cutting the peptide fragments. The feasibility of chopping the SAP fibres by ultrasound was previously demonstrated by Zhang's group. The SAP sample was treated using ultrasound with a fixed treatment time and the dynamic reassembly of the chopped segments generated fibres with different lengths.[21] We show here that the SAP nanomillipede length can be simply tuned by sonicating the nanomillipede sample for 0 min, 15 min, and 30 min in an ice bath in an ultrasonic cleaner (Powersonic P1100D-45, maximal power setting). The TEM samples were prepared immediately after ultrasonic treatment. The number of nanomillipedes increased while the average length decreased linearly upon increasing the ultrasound treatment time (Fig. 2b–e). The aspect ratio of the nanomillipedes decreased to 60% (Fig. 2e, grey line).

To test the stability of the fragmented nanomillipedes, we added the ultrasound-treated (30 min) nanomillipedes into a buffer containing 50 vol% glycerol, mimicking the hydrogel precursor milieu in terms of viscosity[22] while allowing the imaging of nanostructures. After 0 h, 12 h and 48 h incubation, there was no significant change in their length (Fig. S16, ESI†). The time frame being investigated is already much longer than that of the gelation process, which is completed within 5 min.

The preformed mature nanomillipedes were used as the crosslinkers to prepare hybrid hydrogels. The gelation condition was examined by an inverted vial test (Table S1, ESI†). Only nanomillipedes with peptide concentrations higher than 2 mM result in the formation of a hybrid hydrogel network (Exp. 1–Exp. 6). The coexistence of the VS reaction sites on the dextran backbone (Exp. 7 and Exp. 8) and the SH reaction sites on the nanomillipedes (Exp. 9 and Exp. 10) is required for the formation of the crosslinked hybrid network and further gelation. The necessity of an ordered microscopic structure of nanomillipedes for gel formation was

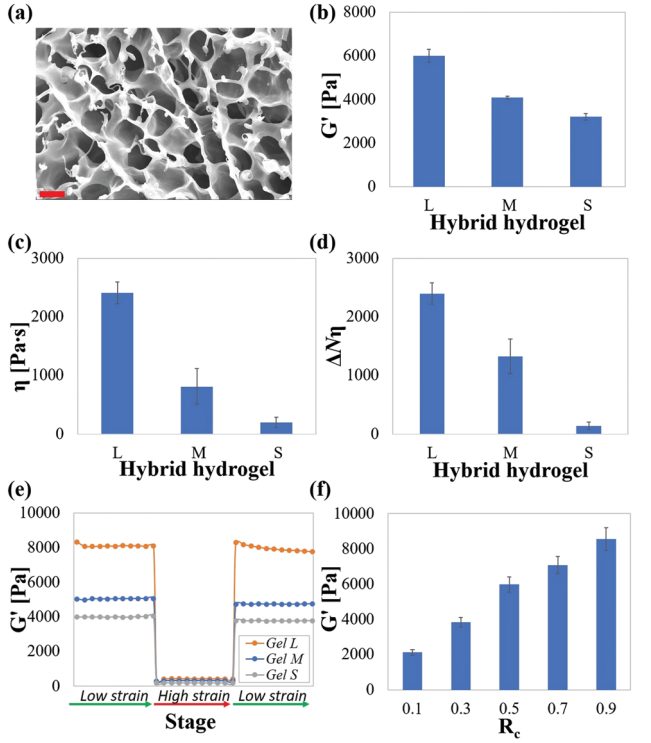

Fig. 3 Tuneable dextran/peptidic nanomillipede hybrid hydrogel characterization. (a) SEM image. Scale bar: 10 μm. (b) Tuneable mechanical strength. (c) Tuneable viscosity. (d) Tuneable shear-thinning property. (e) Step-strain measurement. (f) Tuning mechanical strength by varying R_c value. Gel 'L', Gel 'M' and Gel 'S' represent hybrid hydrogels prepared from long (no ultrasound), medium (15 min ultrasound treatment), and short (30 min ultrasound treatment) nanomillipedes, respectively.

supported by the absence of gel formation when the experiments were conducted using the scrambled SAP mixture (Exp. 11). These series of experiments showed that the VS-Dex polymer backbone is crosslinked by the peptidic nanomillipede crosslinkers to form the hybrid hydrogel network.

The microscopic morphology of the dextran-peptide hybrid hydrogel was characterized by scanning electron microscopy (SEM) and the result indicates a regular honeycomb-like porous structure (Fig. 3a and Fig. S17, ESI†). This honeycomb-like morphology presents a more uniform structure compared with previously reported peptide–polymer hybrid hydrogel systems.[23,24] The homogenous micropores with high continuity[25] within the hybrid hydrogel crosslinking network are around 10 μm size, which may favour the migration of cells and nutrients into the hydrogel scaffold.[2]

ATR-FTIR was used to characterize the secondary structure of the peptidic nanomillipede crosslinker within the hybrid hydrogel system. For a hybrid hydrogel, the peak near 1625 cm^{-1} (amide I stretch peak) and the shoulder near 1695 cm^{-1} indicate the antiparallel β-sheet architecture of the incorporated peptidic nanomillipede crosslinker[16] (Fig. S18, ESI†). This result is in agreement with the ATR-FTIR result of the nanomillipede crosslinkers alone, thereby indicating that the secondary structure of the peptidic nanomillipede crosslinkers remains intact after being incorporated into the hybrid hydrogel network. By contrast, the co-incubation of the VS-modified dextran and the scrambled SAP mixture cannot result in hydrogel formation and the peak near 1640 cm^{-1} indicates a random coil architecture (Fig. S19, ESI†).[18] This confirms that the hybrid hydrogel network is crosslinker conformation-dependent, and only the peptide self-assembly with ordered microscopic structure can result in crosslinking and further gelation.

The mechanical properties of hybrid hydrogels were studied by dynamic mechanical analysis (DMA). The dynamic strain sweep test shows that the storage modulus (G') is higher than the loss modulus (G'') and $\tan\delta$ ($\tan\delta = G''/G'$) is much lower than 1 across a wide strain (γ) range, which indicates that the elastic property is dominant over the viscous property. The elastic hybrid hydrogel appears to form when γ exceeds 30% ($G' < G''$), thereby indicating structural disruption within the crosslinked hydrogel network (Fig. S20, ESI†). The hydrogel-like elastic property was also supported by the frequency sweep test across the whole range of angular frequencies (0.1–100 rad s^{-1}, γ = 2%, Fig. S21, ESI†).

The dynamic frequency sweep test was also carried out to characterize the shear stress change and viscosity change as a function of shear rate (γ'). The viscosity decreases over three orders of magnitudes with the increase of the shear rate, which indicates prominent non-Newtonian shear-thinning (pseudoplastic) behaviour (Fig. S22, ESI†). We reason that the prominent shear-thinning behaviour originates from a combination of mechanical disruption and shear-induced realignment. First, the hydrogel is a semi-liquid fluid system, which differs from liquid fluid where the viscosity originates from the friction between the fluid molecules.[26] The shear stress results in partial disruption of the intermolecular physical interactions within the peptide nanomillipede crosslinker, while the dynamic reassembly-based crosslinker recovery process lags the shearing process. Second, steady shear stress initiates localized microflow, which results in the realignment of the high aspect-ratio peptidic nanomillipedes. This realignment process will, in turn, diminish the shear resistance and facilitate the shearing process. This property is especially beneficial for therapeutic cargo encapsulation under constant conditions and facile injection through high gauge needles.[27,28]

Step-strain measurement was carried out to investigate the self-healing properties. This measurement contains alternative low strain (2%) and high strain (150%) measurement, which represent the normal strain sweep test and high strain disruption, respectively. The low strain measurement was carried out again after 30 min recovery period and prominent increase in G' was observed. The recovered G' is at least 95% of the original G', which indicates rapid and efficient self-healing property (Fig. S23, ESI†). A possible mechanism of the self-healing process is illustrated in Fig. S24 (ESI†). When the material yields, the reversible intermolecular physical interactions are partially disrupted while the chemical bonds remain intact. The reassembly of the disrupted nanomillipedes enables the healing of the hydrogel network, and is possible when the proximity of the damaged nanomillipedes are facilitated by local displacement derived from disruption.

Then, we tested the influence of the length dimension of the nanomillipede crosslinkers on the mechanical properties of hybrid peptide–polymer hydrogels (Fig. S25, ESI†). About 47% decrease in the storage modulus (G') was observed for the hybrid hydrogel prepared from the 30-min ultrasound treated crosslinkers (Fig. 3b, γ = 2%, ω = 10 rad s^{-1}, n = 3). Different from the reported mechanical tuning method, the chemical compositions and components remain unchanged in this work. The hybrid hydrogel network is formed through crosslinking by thiol-containing nanomillipedes. Ultrasound pretreatment will result in tuning of the length of the nanomillipedes without changing the overall number of the chemical crosslinking density of the hybrid network. Longer nanomillipedes within the hybrid hydrogel system provide more non-covalent intermolecular interactions, which are more resistant to external mechanical forces and generate stronger hydrogels.

The tuneable shear-thinning property was characterized by a viscosity change in the dynamic frequency sweep test (Fig. S26, ESI†). The viscosity (at low frequency) decreased by 92% (Fig. 3c, γ = 2%, ω = 0.1 rad s^{-1}, n = 3) and viscosity attenuation factor (ΔN_η, low-frequency viscosity divided by high-frequency viscosity, defined in eqn (S1), ESI†) decreased by 94% (Fig. 3d, γ = 2%, n = 3). This is in agreement with the proposed hypothesis for the shear-thinning mechanism. At low frequency, the alignment effect is minimal, and the viscosity is mainly derived from the physical entanglement of the nanomillipedes. Longer nanomillipedes provide more physical entanglement and generate higher viscosity (Fig. 3c). With the increase in frequency, the alignment effect turns prominent. The high aspect-ratio nanomillipede crosslinkers appear to align lengthwise toward the directions of shear stress to minimize the interlamellar shear-stress. Nanomillipedes with higher aspect-ratio have more prominent alignment effect, thereby generating more prominent shear-thinning properties (Fig. 3d).

The step-strain measurement was carried out for hybrid hydrogels prepared from nanomillipedes with different length, and the result shows all hybrid hydrogels exhibit efficient self-healing property, (Fig. 3e) which is also reversible and can be cycled (Fig. S27, ESI†).

The mechanical properties of the hybrid hydrogel were also tuned by varying the reactive thiol group density on the nanomillipede crosslinkers. Nanomillipedes with the same peptide concentration but different ratio of cysteine-containing peptide (R_c) value (defined in eqn (S3), ESI†) were used to construct hybrid hydrogels. The results (Fig. S28 and Fig. 3f, γ = 2%, ω = 10 rad s^{-1}, n = 3, ESI†) show that a higher R_c value gives rise to a stronger gel. This is because a higher R_c value represents a higher density of the reaction sites for crosslinking, thereby generating a more densely crosslinked hybrid gel network and stronger gels.

In conclusion, a peptidic nanomillipede-based dextran hybrid hydrogel is synthesized. This new hybrid system incorporates both chemical crosslinking and physical intermolecular interactions, which provide soft-tissue mimicking mechanical strength and reversible properties (injectable, self-healing and shear-thinning properties), respectively. What's more, the length of the peptidic nanomillipede can be simply tuned by controlling the ultrasound treatment time, and the mechanical properties of gels can be further tuned. All these features endow this hybrid hydrogel with promise as a new biomaterial platform for expanding its applications in tissue engineering and drug delivery.

Financial support was provided by the Hong Kong Research Grant Council (GRF 16103517 and GRF 16306917) and the Hong Kong PhD Fellowship Scheme (for Jianhui Liu).

Conflicts of interest

There are no conflicts to declare.

References

1 J. L. Drury and D. J. Mooney, *Biomaterials*, 2003, **24**, 4337–4351.
2 S. Yang, K.-F. Leong, Z. Du and C.-K. Chua, *Tissue Eng.*, 2001, **7**, 679–689.
3 A. J. Engler, S. Sen, H. L. Sweeney and D. E. Discher, *Cell*, 2006, **126**, 677–689.
4 C. Fan, L. Liao, C. Zhang and L. Liu, *J. Mater. Chem. B*, 2013, **1**, 4251–4258.
5 K. Y. Lee, J. A. Rowley, P. Eiselt, E. M. Moy, K. H. Bouhadir and D. J. Mooney, *Macromolecules*, 2000, **33**, 4291–4294.
6 L. Haines-Butterick, K. Rajagopal, M. Branco, D. Salick, R. Rughani, M. Pilarz, M. S. Lamm, D. J. Pochan and J. P. Schneider, *Proc. Natl. Acad. Sci. U. S. A.*, 2007, **104**, 7791–7796.
7 D. M. Raymond and B. L. Nilsson, *Chem. Soc. Rev.*, 2018, **47**, 3659–3720.
8 R. Ni, J. Liu and Y. Chau, *RSC Adv.*, 2018, **8**, 29482–29487.
9 E. Radvar and H. S. Azevedo, *Macromol. Biosci.*, 2018, **19**, 1800221.
10 I. Levental, P. C. Georges and P. A. Janmey, *Soft Matter*, 2007, **3**, 299–306.
11 C. M. Rubert Pérez, L. A. Rank and J. Chmielewski, *Chem. Commun.*, 2014, **50**, 8174–8176.
12 P. J. Stahl, N. H. Romano, D. Wirtz and S. M. Yu, *Biomacromolecules*, 2010, **11**, 2336–2344.
13 L. C. Wu, J. Yang and J. Kopeček, *Biomaterials*, 2011, **32**, 5341–5353.
14 D. E. Clarke, E. T. Pashuck, S. Bertazzo, J. V. M. Weaver and M. M. Stevens, *J. Am. Chem. Soc.*, 2017, **139**, 7250–7255.
15 L. C. Radu-Wu, J. Yang, K. Wu and J. Kopeček, *Biomacromolecules*, 2009, **10**, 2319–2327.
16 E. Goormaghtigh, J. M. Ruysschaert and V. Raussens, *Biophys. J.*, 2006, **90**, 2946–2957.
17 C. M. Bishop, W. F. Walkenhorst and W. C. Wimley, *J. Mol. Biol.*, 2001, **309**, 975–988.
18 G. S. Perrone, G. G. Leisk, T. J. Lo, J. E. Moreau, D. S. Haas, B. J. Papenburg, E. B. Golden, B. P. Partlow, S. E. Fox, A. M. S. Ibrahim, S. J. Lin and D. L. Kaplan, *Nat. Commun.*, 2014, **5**, 1–9.
19 N. J. Greenfield, *Nat. Protoc.*, 2007, **1**, 2876–2890.
20 A. Vallée-Bélisle and S. W. Michnick, *J. Mol. Biol.*, 2007, **374**, 791–805.
21 H. Yokoi, T. Kinoshita and S. Zhang, *Proc. Natl. Acad. Sci. U. S. A.*, 2005, **102**, 8414–8419.
22 R. Li, A. J. D'Souza, R. L. Schowen, R. T. Borchardt, E. M. Topp and B. B. Laird, *J. Pept. Res.*, 2000, **56**, 326–334.
23 Y. Hao, A. B. Zerdoum, A. J. Stuffer, A. K. Rajasekaran and X. Jia, *Biomacromolecules*, 2016, **17**, 3750–3760.
24 M. Guvendiren, H. D. Lu and J. A. Burdick, *Soft Matter*, 2012, **8**, 260–272.
25 D. J. Mooney, D. F. Baldwin, N. P. Suh, J. P. Vacanti and R. Langer, *Biomaterials*, 1996, **17**, 1417–1422.
26 S. E. Quiñones-Cisneros, C. K. Zéberg-Mikkelsen and E. H. Stenby, *Fluid Phase Equilib.*, 2000, **169**, 249–276.
27 E. A. Appel, M. W. Tibbitt, M. J. Webber, B. A. Mattix, O. Veiseh and R. Langer, *Nat. Commun.*, 2015, **6**, 1–9.
28 S. K. Seidlits, Z. Z. Khaing, R. R. Petersen, J. D. Nickels, J. E. Vanscoy, J. B. Shear and C. E. Schmidt, *Biomaterials*, 2010, **31**, 3930–3940.

